JOURNAL OF SPACECRAFT AND ROCKETS
Vol. 30, No. 3, May–June 1993

Mach 10 Bow-Shock Behavior of a Forward-Facing Nose Cavity

Lawrence D. Huebner*
NASA Langley Research Center, Hampton, Virginia 23665
and
Lajpat R. Utreja†
Dynacs Engineering Company, Inc., Huntsville, Alabama 35806

A detailed description of the bow-shock behavior associated with a conical-walled cavity with a flat circular base at $M_\infty = 10$ is presented. An experimental test was performed on this configuration, and measurements of shock-oscillation frequency and amplitude, as well as shock shape, were recorded by a number of techniques, one being a laser-interferometer system used for the first time during this test to determine bow-shock oscillation frequency in a nonintrusive manner. The primary behavior was a stable, periodically oscillating bow shock. Discussions are also made on a violent bow-shock instability that occurred for one set of conditions during the test.

Nomenclature

M_∞ = freestream Mach number
$\dot{m}$ = mass-flow rate, lbm/s
Re_∞ = freestream Reynolds number, 1/ft
α = angle of attack, deg

Introduction

A NOVEL hollow-nosed missile concept conceived as a passive means of significantly reducing the heat flux in a forward-facing cavity has been recently investigated.[1] One of the characteristics of a hollow-nosed missile at supersonic Mach numbers is an oscillating bow shock that can significantly influence missile drag, heat transfer, and optical signal propagation through the cavity. It has been reported in the literature[2–4] that the stagnation-point heat transfer coefficient of a concave hemispherical nose (i.e., nose cavity) at various supersonic and hypersonic Mach numbers is anywhere from 2 to 10 times less than that of a convex hemispherical nose. This fact can be used in the nose design by centrally locating a forward-looking sensor at the base of a forward-facing cavity. In so doing, the heat transfer to and temperature rise of the window material may be reduced enough for some applications to eliminate the need for active cooling.

Previous experimental studies[2–5] of concave nose configurations in supersonic and hypersonic flow indicate that the disturbed flow can either be steady or unsteady, depending on various conditions. Cooper et al.[3] noticed that, for angles of attack less than approximately 2 deg at $M_\infty = 1.98$ and 4.95, the flow alternated in a random manner from steady flow (fixed shock position) to unsteady flow (oscillating bow shock). Furthermore, the stagnation-point heat transfer coefficient was six to seven times higher for this unsteady flow as compared with the steady flow. For angles of attack greater than 2 deg, the flow was steady. Stallings and Burbank[4] also obtained both steady and unsteady flowfields in the range of $M_\infty = 2.94$–4.44. The unsteady flow, characterized by unpredictable, sporadic bow-shock behavior, was more predominant at small angles of attack and higher Mach numbers. Johnson[5] made studies at $M_\infty = 22$ in helium on a number of cavity shapes and observed that, for cylindrical and conical cavities, the bow shock was steady. However, if gas was injected into the stagnation region of the cavity, violent flowfield instability and an unsteady bow shock resulted.

Several computational studies[6–8] have been performed on concave configurations. Bastianon[6] found that, at $M_\infty = 3$ for cavity depths greater than 40% of the cylindrical body radius, the viscous solution is unsteady and the flow generates an undamped, cyclically repeating oscillating wave. Bohachevsky and Kostoff[7] found that the flow about a conical cavity at $M_\infty = 5$ has initial shock oscillations that are strongly damped and eventually reach a nonoscillatory condition. They further investigated a thin-walled hollow cylinder at $M_\infty = 10$ incorporating artificial viscosity and found that the shock once again exhibited damped oscillations before eventually reaching a steady-state position. They also noted that the shock oscillation frequency was related to the distance from the cavity base to the shock equilibrium position. Sambamurthi et al.[8] investigated a two-dimensional conical-walled cavity with a flat base at $M_\infty = 10$ using a time-dependent Navier-Stokes code. Their results predicted a shock that oscillated at a frequency corresponding approximately to the fundamental acoustic frequency of the cavity, with a wavelength that was four times the distance from the cavity base to the mean shock position.

In the present study, the unsteady nature of the flowfield associated with a conical-walled cavity with a flat circular base at $M_\infty = 10$ was investigated experimentally in a wind-tunnel test. The objectives of the test were 1) to make detailed observations of bow-shock behavior; 2) to measure bow-shock dynamics, using dynamic pressure response in the cavity, high-speed movies, and a laser-interferometer system to determine acoustic characteristics of the cavity; 3) to study the effects of scaling on bow-shock behavior; and 4) to study methods to improve bow-shock stability by injecting air into or evacuating air from the cavity. The purpose of this paper is to discuss in detail the bow-shock behavior of this cavity, as measured by a number of different techniques. This behavior includes shock-oscillation frequency and amplitude, as well as shock shape. Discussions are also made on the violent bow-shock instability that occurred for one set of conditions during the test.

Model Description

The wind-tunnel test of this concept concentrated primarily on a 50% scale model configuration. This model with its three parts—nose, midbody, and aftbody—is shown in Fig. 1 along with pertinent dimensions. Because of limitations on tunnel size and concerns about tunnel blockage at extreme angles of attack, the aft external characteristics of the test article did not duplicate that of the baseline missile configuration (Fig. 2). A forward-looking sensor will generally be located at the base of the cavity behind the

Received Oct. 15, 1991; revision received Aug. 17, 1992; accepted for publication Oct. 2, 1992.

*Aerospace Engineer, Hypersonics Group Leader, Supersonic/Hypersonic Aerodynamics Branch, Applied Aerodynamics Division, MS 413. Senior Member AIAA.

†Director, Huntsville Division, 150 West Park Loop, Suite 305. Associate Fellow AIAA.

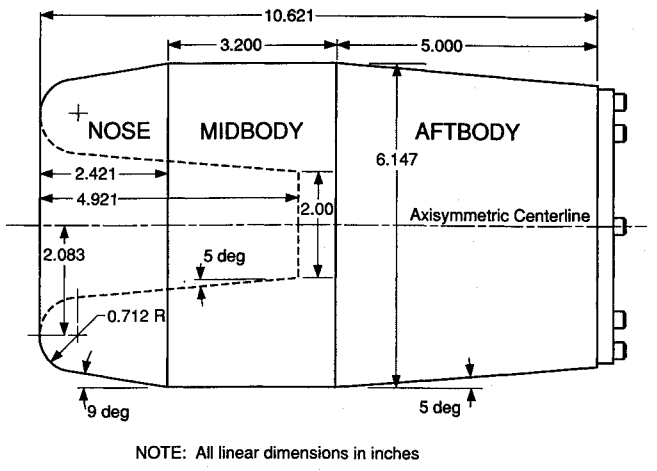

Fig. 1 Configuration and dimensions of 50% scale model.

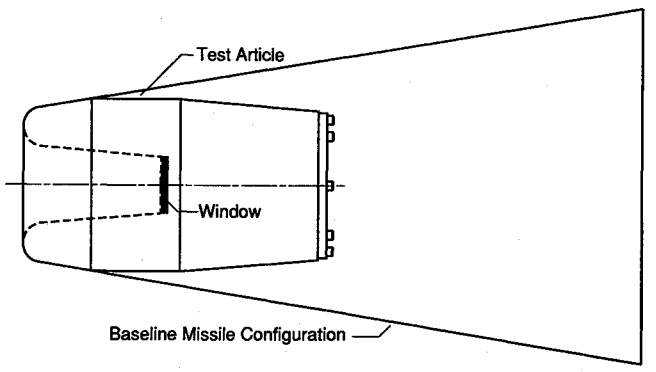

Fig. 2 Comparison of test article with baseline missile configuration.

window in the missile configuration shown in Fig. 2. However, the objective of the test was to study flowfield features in and around the cavity. The sonic line at test conditions was expected to be on the nose portion of the model so that the external airflow on the midbody and aftbody will not propagate upstream influencing the cavity flow.

The three model configurations that were tested are shown in Fig. 3. Two of these configurations were the 50% scale, deep and shallow cavities. The terms deep and shallow are used here to make a distinction between the two cavities and make no reference to their aspect ratios. The 50% scale, deep-cavity configuration discussed previously is shown at the top of the figure. During test runs in which air was evacuated from or injected into the cavity, the four flow ports on the midbody were opened, one of which is shown in cutaway. The 50% scale, shallow-cavity configuration, Fig. 3, middle, was derived by removing the midbody and mating the nose directly to the aftbody. The 75% scale, deep-cavity configuration, Fig. 3, bottom, consisted of a solid nose piece attached to the common aftbody. Since the midbody was removed for both of the last two configurations, mass injection or evacuation could not be performed on these models.

For the purpose of this paper, dynamic pressure transducers were the only pertinent model instrumentation. Location of working dynamic pressure transducers, as well as mass-flow ports described earlier, are shown in Fig. 3, top. The transducers were located on the vertical symmetry plane, whereas the mass-flow ports were ±45 deg off the vertical symmetry plane. Dynamic pressure response was used to correlate acoustic characteristics with bow-shock oscillation frequency. The ultra-miniature dynamic pressure transducers used on this model had a 0–15 psia pressure range accurate to ±1% at full scale and a useful frequency range of 0–25 kHz. Information on the other instrumentation used during the test as well as model drawings can be found in Ref. 9.

Test Description

This test was conducted in the von Kármán Gas Dynamics Facility (VKF) in the Hypersonic Wind Tunnel C at the Arnold Engineering Development Center (AEDC), Tullahoma, Tennessee. Tunnel C is a closed-circuit wind tunnel with a Mach number 10 axisymmetric contoured nozzle and a 50-in. test section. The tunnel is equipped with a model injection system, which allows removal of the model from the test section while the tunnel remains at run conditions.[10] Test conditions included a freestream Mach number of 10, Reynolds numbers of 1.1 and 2.2×10^6/ft, and angles of attack between ±10 deg. During test runs that included air injection into the cavity, the mass-flow rates varied from 0.33 to 4.2×10^{-3} lbm/s, whereas air evacuation was performed at about 0.67×10^{-3} lbm/s.

Shock oscillation analysis was performed using two types of data. Shock shape, standoff distance, and oscillation amplitudes were obtained from high-speed movies that were recorded at rates up to 9000 frames/s. A motion analyzer was used to determine shock shape and to measure the time-dependent shock-standoff distance that yielded mean standoff distance and rms amplitude for runs in which film was taken. A method for determining bow-shock oscillation frequency in a nonintrusive manner was used for the first time at AEDC during this test. It consisted of a modified boundary-layer transition detector (BLTD), originally developed at AEDC for turbulence measurements.[11] The system (Fig. 4) consisted of a 5-MW He-Ne laser and a block beam splitter that separated the laser beam into two beams of equal intensity (one beam positioned in the freestream ahead of the bow shock and the other penetrated the oscillating bow shock). The two beams were then superimposed, forming a fringe pattern on a retroreflector surface, and the light intensity fluctuations caused by the oscillating bow shock were sensed by a photo detector. These data were digitized

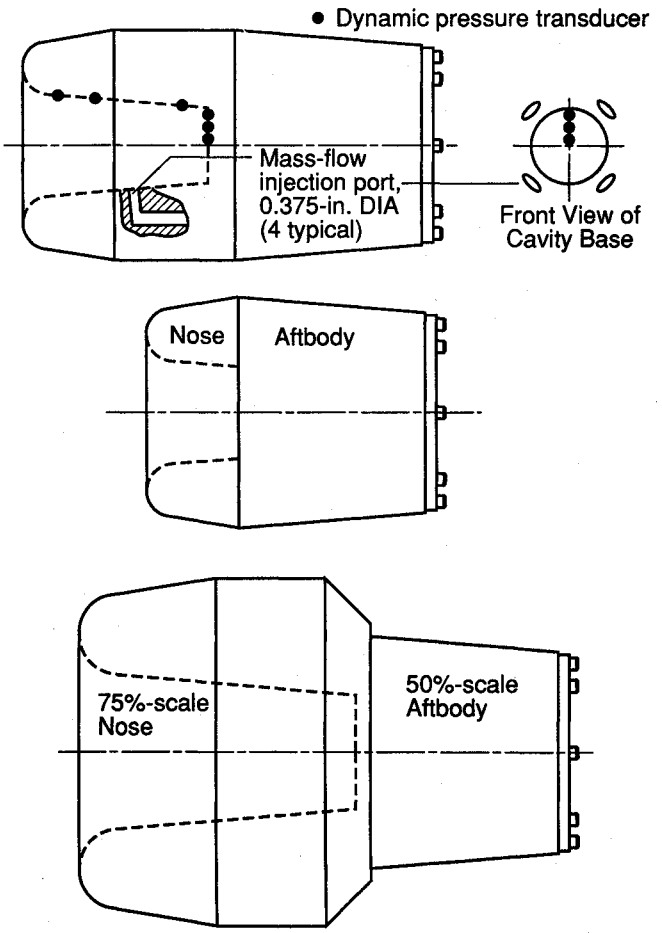

Fig. 3 Wind-tunnel model configurations, including injection port and dynamic pressure transducer locations.

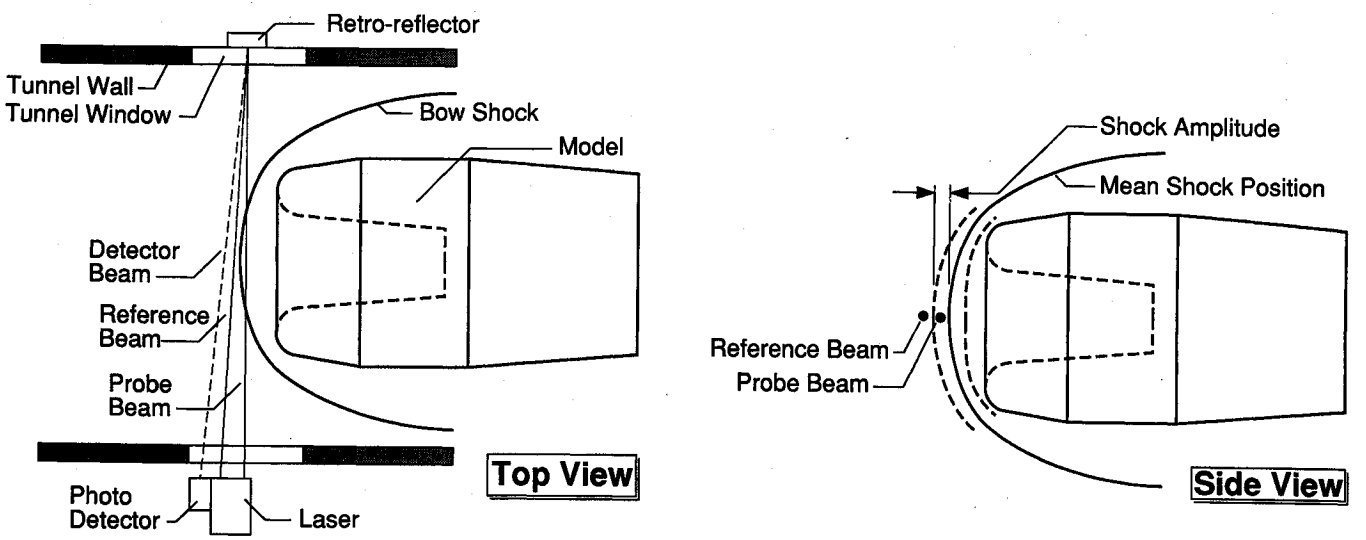

Fig. 4 Boundary-layer transition detector modified for shock-oscillation frequency measurements.

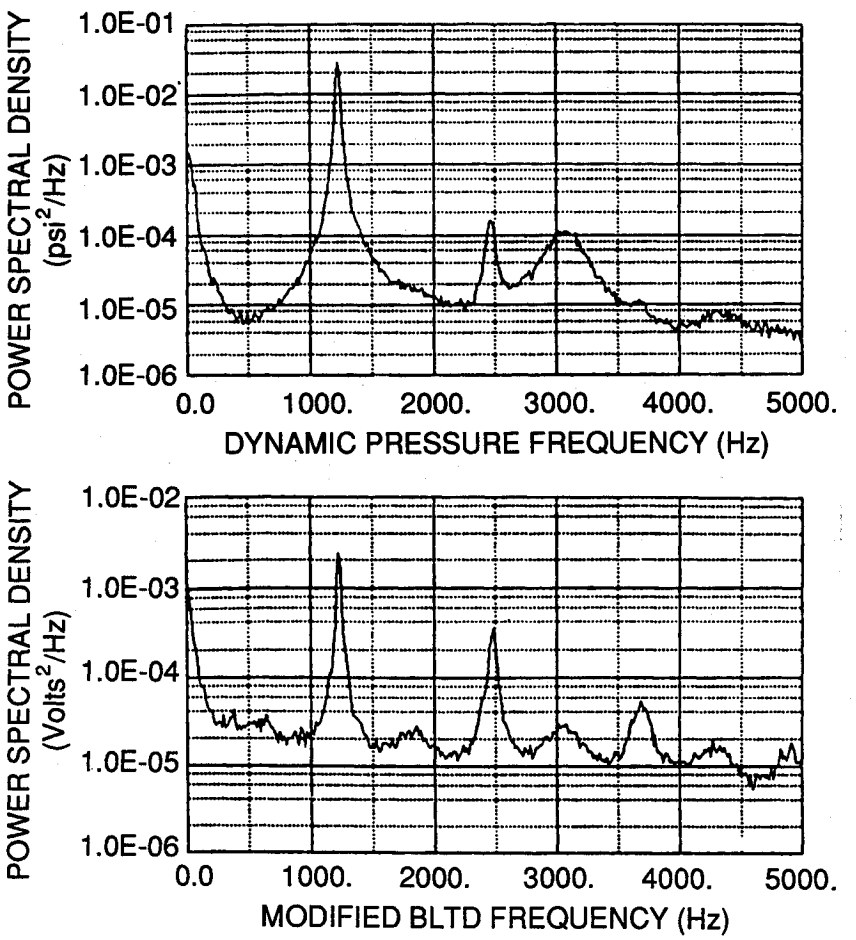

Fig. 5 Autospectral comparison of shock-oscillation frequency measurement systems, 50% scale, deep-cavity configuration, $M_\infty = 10$, $Re_\infty = 2.2 \times 10^6$/ft, $\alpha = 0$ deg, no mass injection.

and their autospectra computed using a spectrum analyzer to obtain plots of relative energy as a function of frequency.

Experimental Results

In every run during the test, the bow shock oscillated. The oscillatory behavior was observed on video monitors during the test, and the oscillation amplitudes were shown to be less than the shock-standoff distance from the nose rim. Discussions of self-sustained flow oscillations appear in the literature.[12,13] For this study, the mechanism controlling the oscillation is thought to result from a nonuniform stagnation pressure distribution behind the shock. This results in an unstable flow pattern inside the cavity because mass conservation cannot be established there, leading to a periodic charging and discharging of the cavity. The process includes pressure oscillation in the cavity and shock oscillation in front of it.

The time-dependent bow-shock geometric data were obtained by analyzing the high-speed film one frame at a time for at least 100 frames once the operating frame rate of the film was achieved. The frequency of the oscillating bow shock was determined from

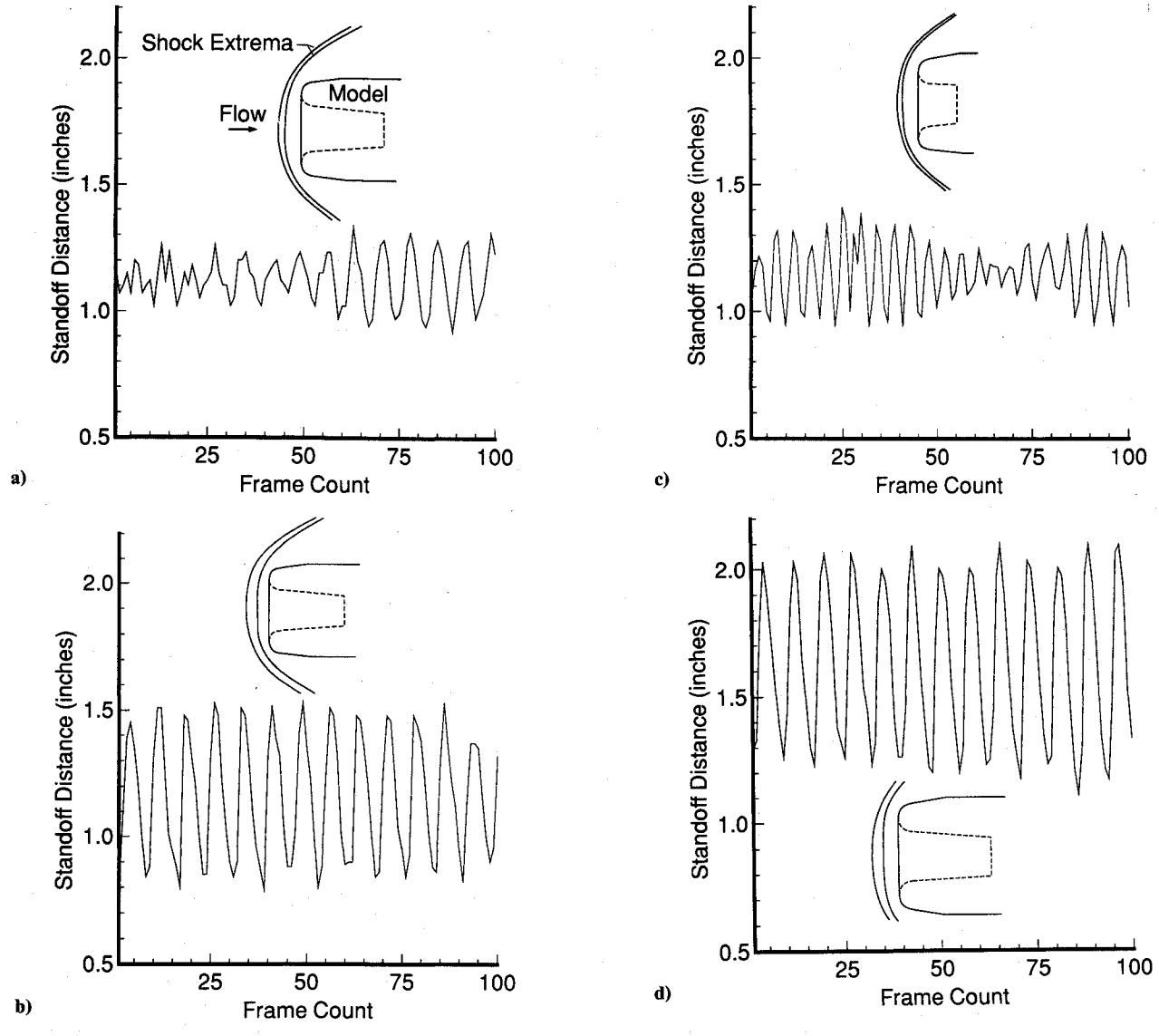

Fig. 6 Shock data for forward facing cavity configurations with no mass injection, $M_\infty = 10$, $\alpha = 0$ deg: a) 50% scale, deep cavity, $Re_\infty = 2.2 \times 10^6$/ft, film speed ≈9000 frames/s; b) 50% scale, deep cavity, $Re_\infty = 1.1 \times 10^6$/ft, film speed ≈8400 frames/s; c) 50% scale, shallow cavity, $Re_\infty = 1.1 \times 10^6$/ft, film speed ≈8400 frames/s; d) 75% scale, deep cavity, $Re_\infty = 2.2 \times 10^6$/ft, film speed ≈6600 frames/s.

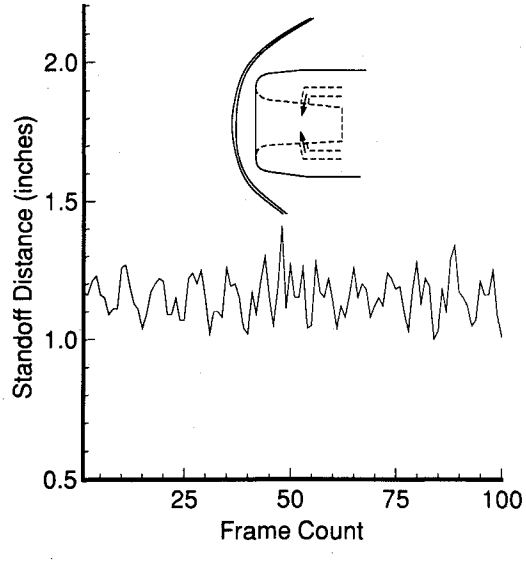

Fig. 7 Shock data for 50% scale, deep cavity configuration with mass injection, $M_\infty = 10$, $Re_\infty = 1.1 \times 10^6$/ft, $\alpha = 0$ deg, $\dot{m} = 1.036 \times 10^{-3}$ lbm/s, film speed ≈8400 frames/s.

the autospectra of the data from the dynamic pressure transducers and the modified BLTD. A representative comparison of the results from these two methods is shown in Fig. 5 for the 50% scale, deep-cavity configuration at 0 deg angle of attack and a Reynolds number of 2.2×10^6/ft. Both autospectra yielded a fundamental shock-oscillation frequency of 1230 Hz, providing a 95% coherence at that frequency. The phase-angle comparison (not shown) indicated that the bow-shock motion detected by the modified BLTD lags the oscillating dynamic pressure by about 120 deg at the fundamental frequency. This implies that the mechanism that causes pressure fluctuations inside the cavity is driving the bow-shock oscillations.

Bow-Shock Behavior (Periodic Oscillations)

Figures 6 and 7 present shock data for all three configurations and effects due to Reynolds number and mass injection. Each plot shows shock standoff distance (with comparable scales) as a function of frame count (time) and an accurate sketch of the shock shape extremes for each case. In general, results indicate that bow shock was symmetric with the centerline, always convex, and never attached to the body. Furthermore, all drawings show shock shapes that are almost parallel to the plane of the nose rim, which is a favorable quality if an electromagnetic sensor is located at the cavity base. Figure 6 show results from the three configurations with no mass injection, whereas Fig. 7 presents the results with

mass injection. The standoff distance histories all show the periodicity observed in the autospectral plots (shown in Fig. 5).

Figures 6a and 6b show results for the 50% scale, deep-cavity configuration, analyzed with respect to varying Reynolds number. Decreasing Reynolds number has the effect of increasing shock-standoff distance slightly and the amplitude by approximately a factor of 1.5. Furthermore, a slight drop in oscillation frequency was observed. Although the results are not shown, pitching the model to $\alpha = -8$ deg had no effect on the mean shock standoff distance, rms amplitude, and oscillation frequency at the model centerline. The shock shapes for the two are quite similar, taking into account the different model orientation to the freestream flow.

For the 50% scale, shallow-cavity configuration (Fig. 6c), the oscillation frequency increases, since the fundamental acoustic frequency of the cavity is inversely proportional to the distance from the cavity base to the mean shock position. Furthermore, the mean shock-standoff distance is the same, and the rms amplitude is half of what it was for the deep cavity, consistent with the fact that the shallow cavity is roughly half the depth of the deep cavity. These trends continue for the 75% scale configuration (Fig. 6d) with respect to oscillation frequency and amplitude. However, mean standoff distance is 40% larger, confirming that standoff distance is a function of nose size and not cavity depth.

The effect of injecting air into the cavity at a very small mass-flow rate (1.036×10^{-3} lbm/s) is shown in Fig. 7. At this rate, the cavity filled with air approximately eight times per second. Although the mean shock-standoff distance and oscillation frequency are the same as if there were no injection (see Fig. 6b for comparison), the rms amplitude with injection is significantly less than with no injection. Furthermore, there is no apparent periodic nature to the standoff-distance history. Insight for this can be seen by comparing autospectra from the two runs, one with injection and the other without (Fig. 8). The second peak in the no-mass-injection autospectra (corresponding to the second harmonic of the fundamental frequency) is two orders of magnitude weaker than the fundamental. In contrast, the mass-injection autospectra shows a secondary peak that is only one order of magnitude weaker than the fundamental and not at an harmonic frequency. Thus, the periodic nature of the run with no mass injection is primarily due to the fundamental frequency, whereas the injection case shows a stand-

Table 1 Summary of shock standoff and oscillation data, $M_\infty = 10$

Configuration	Re_∞, $\times10^6$/ft	α, deg	$\dot{m}$, lbm/s	Mean standoff, in.	Primary frequency, Hz	rms amplitude, in.	Maximum amplitude, in.
50% scale, deep cavity	2.2	0	0.0	1.13	1230	0.10	0.21
50% scale, deep cavity	2.2	−8	0.0	1.13	1220	0.10	0.27
50% scale, deep cavity	1.1	0	0.0	1.16	1140	0.24	0.38
50% scale, deep cavity	1.1	0	0.001036	1.15	1140	0.07	0.19
50% scale, shallow cavity	1.1	0	0.0	1.17	2035	0.12	0.24
50% scale, deep cavity	2.2	0	0.0	1.62	810	0.31	0.51

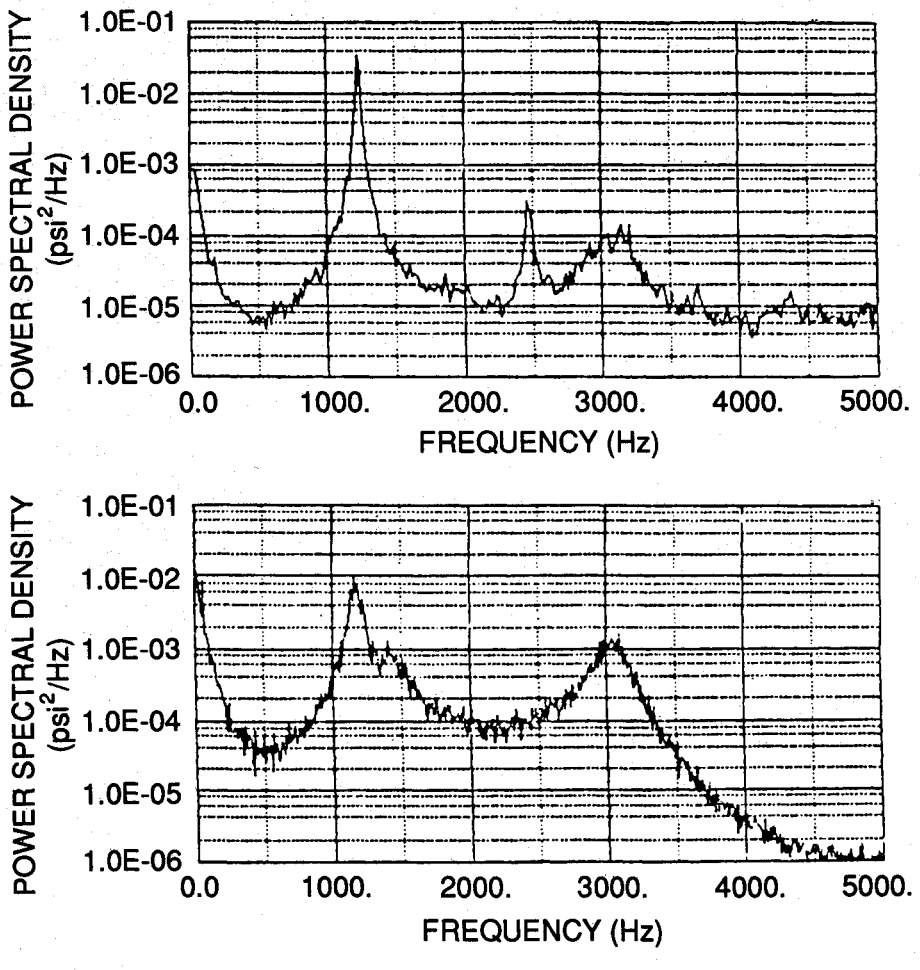

Fig. 8 Autospectra for 50% scale, deep cavity configuration, $M_\infty = 10$, $Re_\infty = 1.1 \times 10^6$/ft, $\alpha = 0$ deg: a) no mass injection; b) mass injection, $\dot{m} = 1.036 \times 10^{-3}$ lbm/s.

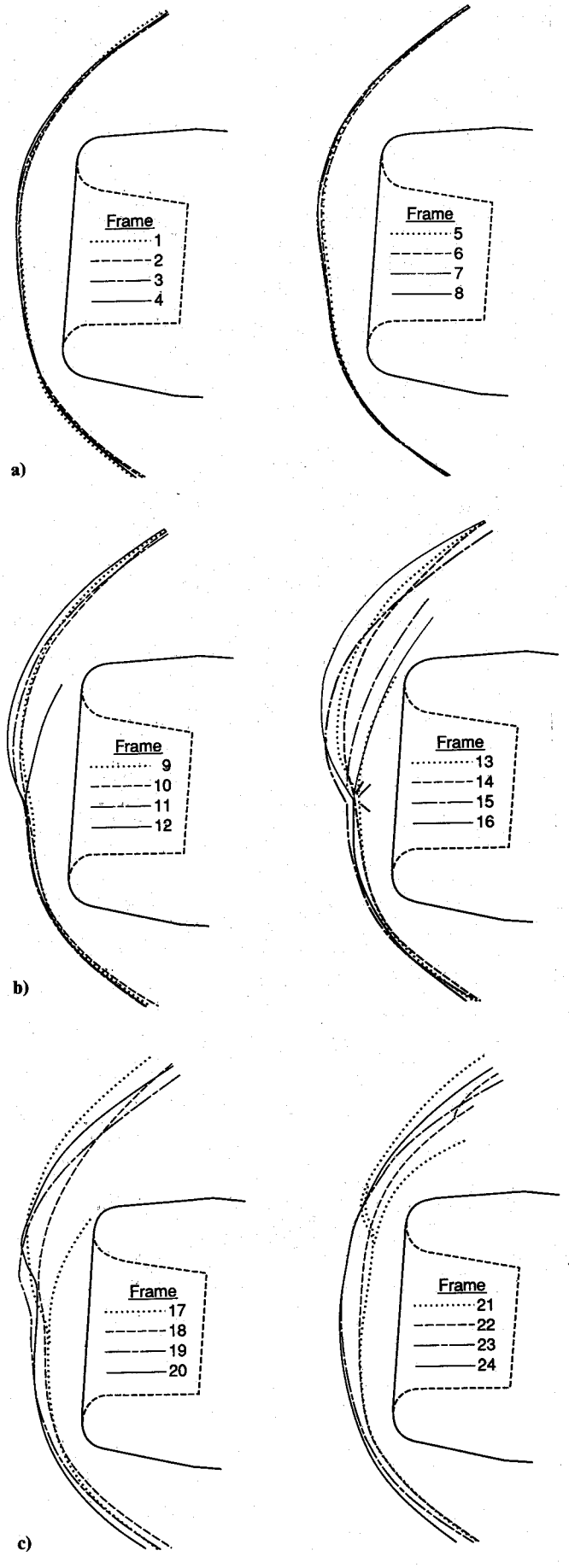

Fig. 9 Sequence showing unstable bow shock motion, 50% scale, shallow cavity configuration, $M_\infty = 10$, $Re_\infty = 2.2 \times 10^6$/ft, $\alpha = 4$ deg, film speed ≈9080 frames/s.

off distance history that includes a superposition of amplitudes from the 1200 and 3000 Hz frequencies. This 3000 Hz frequency has been attributed to a swirl-mode oscillation occurring inside the cavity.[14]

Table 1 summarizes the results of the bow-shock behavior discussed so far. A number of important conclusions can be drawn from these results. First, mean shock-standoff distance was shown to be related to nose size and suggests that the flow sees the nose-cavity configuration as if it possessed a flat face. Reference 15 discusses this in more detail. Second, the frequency of the oscillating shock is inversely proportional to cavity depth and corresponds to the classical interpretation of the fundamental acoustic frequency. Third, varying angle of attack does not significantly alter the shock shape, standoff distance, and amplitude. Last, the oscillating-shock amplitude is directly proportional to Reynolds number for configurations with no mass injection, whereas a significant reduction in shock amplitude is shown for runs with mass injection. This implies that minimal mass injection into the cavity provides a method for mitigating the shock oscillation by suppressing to some extent the internal flow pattern in the cavity, thus improving shock stability.

The last finding is in marked contrast to the results obtained by Johnson[5] which showed that, for a cylindrical cavity at $M_\infty = 22$ in helium, the shock is steady (nonoscillating) and assumes the same shape and location as if it were a flat-ended circular cylinder. However, if a small quantity of helium or air was injected into the same cavity near the stagnation region, erratic and violent motion of the shock was seen, with asymmetric shock shapes that bulge out on one side and then the other. Johnson further postulated a possible cause for the shock instability with air injection to be the vortex formation, vortex growth, and vortex shedding from within the cavity. In addition, he saw no correlation of this instability to the fundamental acoustic frequency of oscillation. In contrast to Johnson's hypothesis, the existence of vortices and their periodic formation and shedding was suggested as a mechanism for shock oscillation by Sambamurthi et al.[8] for test runs employing no air injection. The corresponding shock oscillations did follow the fundamental acoustic frequency.[14] The only effect of injecting or evacuating a small mass flow into or out of the cavity was that it substantially decreased the amplitude of shock oscillations.

Bow-Shock Behavior (Aperiodic Unstable Motion)

In the 24 out of 46 runs in which high-speed movies were taken, one run showed evidence of an unstable bow shock. This run was for the 50% scale, shallow-cavity configuration, $M_\infty = 10$, $Re_\infty = 2.2 \times 10^6$/ft at 4 deg angle of attack. This behavior was sporadic, in that the unstable bow-shock behavior, which extended over a period of one to three bow-shock oscillations, occurred infrequently and at irregular intervals. Most of the high-speed film data for this run showed a periodically oscillating bow shock.

A sequence of line drawings taken directly from movie frames for this case showing this unstable motion is presented in Fig. 9. Each of the six drawings shows four consecutive shock positions. The total sequence of 24 frames shown occurred in about 0.003 s of real time. In frames 1–11, the bow shock was shown to change shape with a noticeable bulge developing in front of the upper half of the cavity. In frames 12–17, the shock appears to have split where the bulge meets with the relatively undisturbed shock location on the lower half. The hypothesis describing this behavior is that the shock is not actually "breaking," but instead is warped due to high-pressure low-speed flow that develops inside the cavity. As the cavity continues to have a pressure increase and then a decrease once in each cycle, more mass gradually builds up within the cavity until it is violently expelled, as this series of shock shapes shows. The secondary shock lines seen behind the more forward shock are most likely due to the density gradients of the warped bow-shock region being high enough on the outer edges of the three-dimensional bulge to appear in the schlieren photograph. In frames 18–22, the shock appears to be regaining its structure until the shock returns to its stable, oscillatory shape in frames 23 and 24.

This type of shock instability occurred several more times throughout the run. The behavior varied both in duration and shock shape. As discussed in the introduction, the occurrence of violent, unstable bow-shock behavior has been reported previously in the literature. In the case of Stallings and Burbank,[4] their unstable flow resulted in bow-shock attachment to the lip of the cavity. In the present study, the bow shock never became attached to the model. The most likely difference in these two results is geometrical. The ratio of the cavity radius at the rim to the cavity rim radius for this geometry is about 2.9 (see Fig. 1). The same ratio for the model of Ref. 4 was 27.3. The model with the larger rim radius ratio was more likely to result in shock attachment there.

This unstable behavior, although violent, is considered to be a second-order effect because it occurred very infrequently compared with the normal oscillatory behavior of the bow shock (the first-order effect). It is not clear whether this anomalous behavior has any physical relevance to the particular flow condition (M_∞ = 10, α = 4 deg, $Re_\infty = 2.2 \times 10^6$/ft, shallow cavity) or to the cavity configuration in general. The reason this instability was not observed for any other set of conditions is currently not known.

Conclusions

A detailed discussion of the bow-shock behavior associated with a conical-walled cavity with a flat circular base at $M_\infty = 10$ is presented. For each of the 46 runs performed during the test, the bow shock oscillated. The oscillation frequency was found to be inversely proportional to cavity depth and corresponds to the fundamental acoustic frequency of the cavity, with a wavelength that was four times the distance from the cavity base to the mean shock position. The mean shock-standoff distance was shown to be a function of the nose size (not cavity depth) and suggests that the flow sees the nose-cavity configuration as if it possessed a flat face. It was further shown that varying the angle of attack did not significantly alter the shock shape, standoff distance, and amplitude. The amplitude of the oscillating shock was found to be directly proportional to Reynolds number and varies from 9 to 21% of the mean shock-standoff distance for runs with no mass injection. When air is injected into the cavity at a very low mass-flow rate, the shock oscillation amplitude is reduced by 70%. This implies that minimal mass injection into the cavity provides a method for improving shock stability. Finally, the violent, unsteady bow-shock behavior shown during one run of the test was documented and discussed.

References

[1]Utreja, L. R., and Gurley, W. H., "Aircraft Hollow Nose Cone," U.S. Patent 4,850,275, BDM International, Huntsville, AL, July 1989.

[2]Hopko, R. H., and Strass, H. K., "Some Experimental Heating Data on Convex and Concave Hemispherical Nose Shapes and Hemispherical Depressions on a 30-degree Blunted Nose Cone," NACA RM L58A17a, March 1958.

[3]Cooper, M., Beckwith, I. E., Jones, J. J., and Gallagher, J. J., "Heat-Transfer Measurements on a Concave Hemispherical Nose Shape with Unsteady-Flow Effects at Mach Numbers of 1.98 and 4.95," NACA RM L58D25a, July 1958.

[4]Stallings, R. L., and Burbank, P. B., "Heat-Transfer and Pressure Measurements of a Concave-Nose Cylinder for a Mach Number Range of 2.49 to 4.44," NASA TM X-221, Oct. 1959.

[5]Johnson, R. H., "Instability of Hypersonic Flow About Blunt Bodies," *Physics of Fluids*, Vol. 2, No. 5, 1959, pp. 526–532.

[6]Bastianon, R. A., "Unsteady Solution of the Flowfield over Concave Bodies," AIAA Paper 68-946, Sept. 1968.

[7]Bohachevsky, I. O., and Kostoff, R. N., "Supersonic Flow over Convex and Concave Shapes with Radiation and Ablation Effects," *AIAA Journal*, Vol. 10, No. 8, 1972, pp. 1024–1031.

[8]Sambamurthi, J. K., Huebner, L. D., and Utreja, L. R., "Hypersonic Flow Over a Cone with Nose Cavity," AIAA Paper 87-1193, June 1987.

[9]Huebner, L. D., "Wind Tunnel Test Plan: Aerothermodynamic Characteristics of the HASP Concept," The BDM Corporation, BDM/H-86-0545-TR, Huntsville, AL, June 1986.

[10]Anon., *Test Facilities Handbook (12th ed.)*, Vol. 3, Arnold Engineering Development Center, von Kármán Gas Dynamics Facility, Arnold, AFS, TN, March 1984.

[11]O'Hare, J. E., "A Nonperturbing Boundary-Layer Transition Detector," Aerophysics Branch, Calspan Corp., AEDC Division, Arnold AFS, TN.

[12]Jungowski, W. M., "Self-Sustained Oscillation of a Jet Impinging upon a Helmholtz Resonator," *Journal of Fluid Mechanics*, Vol. 179, June 1987, pp. 77–103.

[13]Powell, A., "The Sound-Producing Oscillations of Round Underexpanded Jet Impinging on Normal Plates," *Journal of the Acoustical Society of America*, Vol. 83, No. 2, Feb. 1988, pp. 513–533.

[14]Marquart, E. J., Grubb, J. P., and Utreja, L. R., "Bow-Shock Dynamics of a Forward-Facing Nose Cavity," AIAA Paper 87-2709, Oct. 1987.

[15]Huebner, L. D., and Utreja, L. R., "Experimental Flowfield Measurements of a Nose Cavity Configuration," Society of Automotive Engineers, SAE Paper 871880, Warrendale, PA, Oct. 1987.

Gerald T. Chrusciel
Associate Editor